AGU PUBLICATIONS

JGR

Journal of Geophysical Research: Planets

RESEARCH ARTICLE
10.1002/2014JE004770

Key Points:
- We determined the oxygen long-term variability in the Mars upper atmosphere
- We estimated the annual variability of CO_2 partial density with MRO radio data
- The recovered atmospheric model improves MRO orbit determination

Supporting Information:
- Figures S1–S7

Correspondence to:
A. Genova,
antonio.genova@nasa.gov

Citation:
Genova, A., S. Goossens, F. G. Lemoine, E. Mazarico, S. K. Fricke, D. E. Smith, and M. T. Zuber (2015), Long-term variability of CO_2 and O in the Mars upper atmosphere from MRO radio science data, *J. Geophys. Res. Planets*, *120*, 849–868, doi:10.1002/2014JE004770.

Received 26 NOV 2014
Accepted 23 MAR 2015
Accepted article online 26 MAR 2015
Published online 7 May 2015

Long-term variability of CO_2 and O in the Mars upper atmosphere from MRO radio science data

Antonio Genova[1,2], Sander Goossens[2,3], Frank G. Lemoine[2], Erwan Mazarico[2], Susan K. Fricke[4], David E. Smith[1], and Maria T. Zuber[1]

[1]Department of Earth, Atmospheric and Planetary Sciences, Massachusetts Institute of Technology, Cambridge, Massachusetts, USA, [2]NASA Goddard Space Flight Center, Greenbelt, Maryland, USA, [3]CRESST, University of Maryland, Baltimore County, Baltimore, Maryland, USA, [4]SGT, Inc., Greenbelt, Maryland, USA

Abstract We estimate the annual variability of CO_2 and O partial density using approximately 6 years of Mars Reconnaissance Orbiter (MRO) radio science data from August 2006 to January 2012, which cover three full Martian years (from the northern hemisphere summer of 28 to the northern hemisphere summer of 31). These two elements are the dominant species at the MRO periapsis altitude, constituting about 70–80% of the total density. We report the recovered annual cycle of CO_2 and the annual and seasonal cycle of O in the upper atmosphere. Although no other observations are available at those altitudes, our results are in good agreement with the density measurements of the Mars Express Spectroscopy for Investigation of Characteristics of the Atmosphere of Mars, which uses stellar occultations between 60 and 130 km to determine the CO_2 variability, and with the Mars Global Reference Atmospheric Model 2010 for the O annual and seasonal variabilities. Furthermore, the updated model provides more reasonable MRO drag coefficients (C_D), which are estimated to absorb mismodeling in the atmospheric density prediction. The higher content of dust in the atmosphere due to dust storms increases the density, so the C_Ds should compensate for this effect. The correlation between the drag coefficient and the dust optical depth, measured by the Mars Odyssey Thermal Emission Imaging System (THEMIS) instrument, increases from 0.4 to 0.8 with the a priori and adjusted models, respectively. The trend of C_Ds not only confirms a substantial improvement in the prediction of the atmospheric density with the updated model but also provides useful information for local dust storms, near MRO periapsis, that cannot be measured by the opacity level since THEMIS does not always sample the southern hemisphere evenly.

1. Introduction

Investigation of the atmosphere and climate of Mars relies on both in situ and remote sensing measurements, which provide information on its pressure, temperature, and density from the surface to the top of the atmosphere. These data are then compared with and incorporated in models to understand the physical processes that characterize the current Martian climate [*Smith*, 2008].

A variety of different data have been collected to determine properties of the Mars atmosphere. Landers have been used as meteorological platforms, designed to measure humidity, pressure, temperatures, and wind speed to determine the evolution processes, and present state, distribution, and cycling of water and carbon dioxide [*Grotzinger et al.*, 2012]. Spacecraft are usually equipped with dedicated onboard instrumentation for infrared sounding, visible imaging of clouds and dust, radio and UV occultations, and near-infrared spectroscopy. These primary tools for atmospheric observation provide a good coverage for the determination of atmospheric density and temperatures especially in the low and middle atmosphere. The lack of partial and total atmospheric density data in the Mars thermosphere (the region of the upper atmosphere between approximately 120 and 195 km altitude *Valeille et al.* [2009a], where the temperature increases with altitude) and the exosphere (the outermost layer of the atmosphere, above 195 km altitude, from which molecules can escape the Mars' gravitation) significantly affects the accuracy of the atmospheric models at these altitudes. Mars atmospheric models, such as Stewart-87 [*Stewart*, 1987], Drag Temperature Model (DTM)-Mars [*Bruinsma and Lemoine*, 2002; *Rosenblatt et al.*, 2008], and Mars Global Reference Atmospheric Model (Mars-GRAM) [*Justus et al.*, 1996], have been used, among other applications, in orbit determination programs to compute the atmospheric drag acceleration.

The Radio Science Gravity Investigation of the Mars Reconnaissance Orbiter (MRO) mission aims to improve the knowledge of the structure of the static Martian gravitational field and characterize its temporal variability, relevant to the planet's internal dynamics, and the structure and dynamics of the atmosphere [*Zuber et al.*, 2007]. The 7 years of radio tracking data available can potentially be used to recover the seasonal variation of the low-degree zonal gravity coefficients for this purpose. However, the large errors in the atmospheric drag modeling, due to the low MRO altitude (periapsis at 255 km), reduce the benefits of the MRO tracking data. As a result, *Konopliv et al.* [2011] noted that MRO could not be expected to help extend the seasonal gravity monitoring begun with the Mars Global Surveyor (MGS) mission in 1997 and continued by the Mars Odyssey mission.

The strong drag forces acting on the MRO spacecraft have been generally considered as a limiting perturbation for the spacecraft orbit determination. On the other hand, the drag effect provides indirect measurements of the Martian atmospheric density that may be exploited to retrieve the long-term variability of the partial density of the Mars upper atmosphere constituents. For this reason, we implemented the semiempirical DTM-Mars thermosphere model based on the Drag Temperature Model algorithm, originally developed for the terrestrial thermosphere [*Bruinsma and Lemoine*, 2002; *Berger et al.*, 1998] in our orbit determination and geodetic parameter estimation software, GEODYN II, developed and maintained at NASA Goddard Space Flight Center (GSFC) [*Pavlis et al.*, 2013]. The DTM-Mars model provides a convenient way to directly estimate the coefficients that control the atmospheric temperatures and partial densities of each species. The model, indeed, is based on the hypothesis of static diffusive equilibrium of the atmospheric constituents, which is valid in the heterosphere [*Bruinsma and Lemoine*, 2002]. Therefore, the total density is given by the sum of the partial densities, which are expressed as spherical harmonic expansions that reproduce periodic and nonperiodic variations.

In this paper, we directly estimate some of the atmospheric model coefficients from the complete radio data set and we report on the annual and seasonal variabilities of O, which is the major constituent at the MRO periapsis altitude, and the annual variability of CO_2. This analysis includes observations from three Martian years (from August 2006 to January 2012). Furthermore, we processed an additional MRO year (from January 2012 to April 2013) to provide an independent data set for comparison of the predictions of atmospheric density with the a priori and adjusted DTM-Mars models. The updated model provides atmospheric density profiles that may be used to improve general circulation models near 250–300 km altitude. The determination of the O partial density in the upper atmosphere, in particular, can lead to a better understanding of the composition and the dynamics of the Martian upper thermosphere and exosphere. The O to CO_2 ratio, also called atom-to-molecule ratio (noted $r_{a/m}$ in *Valeille et al.* [2010]), represents a critical parameter for the processes shaping the Martian upper atmosphere, such as ion production, plasma heating, and escape loss due to incident pickup ions. The local background densities of these two species regulate directly the production of O_2^+, which is the main ion in the Martian ionosphere and plays a crucial role in the formation of the hot corona [*Valeille et al.*, 2009a].

This paper is structured as follows. In section 2, we discuss the data and the models used in this study to determine precise orbits for MRO. In section 3, we introduce the Mars upper atmospheric modeling, focusing on the estimation of model coefficients. Finally, we will show results in section 4, describing sensitivity analysis, estimation of CO_2 and O annual and semiannual variabilities, and validation of the adjusted model.

2. Data and Methods

2.1. MRO Radio Science Data

MRO was launched on 12 August 2005, and at the end of August 2006 it began providing radio tracking data for the Radio Science Gravity Investigation [*Zuber et al.*, 2007]. More than 7 years of radio tracking measurements have been collected, covering nearly four Martian years. The Doppler shift of the signal measures the spacecraft velocity in the line of sight from Earth (range rate), and the round trip propagation time of the tracking signal gives a measurement of the relative distance between the ground tracking station and the spacecraft (range). This large amount of data allows us to estimate the long-term periodicity of the Martian atmosphere with three complete Mars' years of data, using the remainder for validation purposes. MRO monitors Mars from a quasi-circular polar orbit (the inclination is 92.5°) with a periapsis at 255 km altitude and 82° *S* latitude, which allow MRO to be in a near-frozen orbit [*Cutting et al.*, 1978; *Bowes et al.*, 2003]. The altitude was chosen to make the orbit Sun synchronous, with a fixed crossing time of 3 P.M. at the ascending node, so that

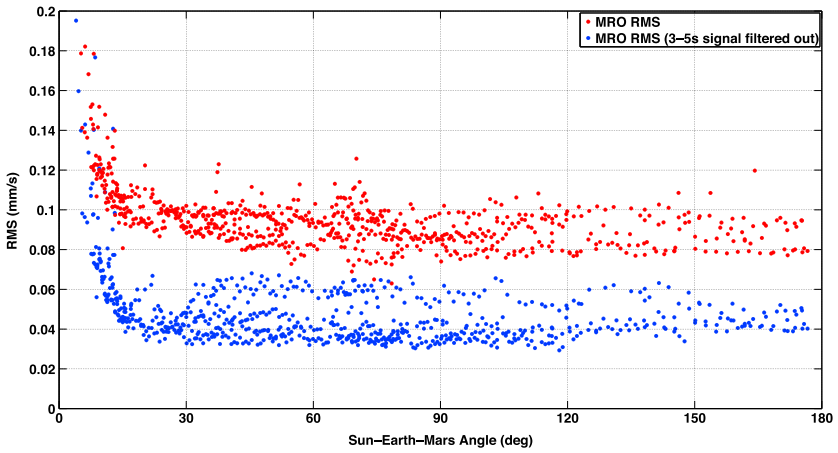

Figure 1. Noise level of the individual tracking passes of MRO, measured as the RMS of the Doppler residuals, as a function of the Sun-Earth-Mars angle. The Doppler data RMS is at 60 s integration time. The red spots are the actual noise of the Doppler data, whereas the blue spots are the RMS after filtering out of the 3–5 s signal.

images are taken under near-ideal lighting conditions. As a consequence, this orbit configuration limits our sensitivity to local solar time and latitudinal variations of the Martian atmospheric constituents.

The MRO tracking data consist of two-way and three-way coherent Doppler data from the Deep Space Network. The difference between two-way and three-way data is that in the first case the signal is transmitted to MRO, transponded coherently back to the Earth and received at the transmitting station. In the case of three-way data, the signal is received at a different station, leading to less accurate measurements. We did not include one-way data in our solution, since the noise of the one-way data is about 5 times greater than the two-way data because of the poor stability of the MRO Ultra-Stable Oscillator compared to the Hydrogen-maser clocks at the ground stations [*Konopliv et al.*, 2011]. The MRO tracking system enables range and range rate measurements at X-band (uplink and downlink frequencies of 7.18 and 8.4 GHz, respectively). A gimbal-steered 3 m diameter high-gain antenna (HGA) and two small deep-space transponders are hosted on board [*Taylor et al.*, 2006]. We modeled the orientation of the spacecraft antenna using the telemetered time-variable inner and outer gimbal angles [*Semenov and Acton*, 2007]. We also tracked the relative position of the MRO HGA with respect to the spacecraft center of mass to account for the apparent line-of-sight velocity due to the HGA motion.

The sensitivity of the Doppler measurements is limited by different error sources, such as thermal noise, solar plasma, and ionospheric and tropospheric delays [*Sniffin et al.*, 2000; *Asmar et al.*, 2005]. The resulting accuracy for MRO is 0.08 mm/s over a 60 s integration time, outside of solar conjunction periods [*Bowes et al.*, 2003; *You et al.*, 2005; *Zuber et al.*, 2007]. We used tracking data TRK2-18 files (http://pds-geosciences.wustl.edu/mro/mro-m-rss-1-magr-v1/mrors_{0}xxx/) for MRO, which provide Doppler data at 1 s integration time. The noise of these data increased by an unknown spacecraft or transponder periodic signature with periods that vary in a range between 3 and 5 s (Figure S1 in the supporting information). Figure 1 shows the typical X-band MRO accuracy for 1 s samples, scaled to 60 s integration time with the purpose to compare it with previous studies [*Zuber et al.*, 2007; *Konopliv et al.*, 2011]. Filtering out the anomalous 3–5 s signal in the Doppler RMS, the noise level decreases significantly to the RMS of 0.04 mm/s. The solutions reported in this paper are achieved with 1 s Doppler data available on the NASA Planetary Data System, which include the 3–5 s signature. However, this high-frequency signal does not affect the estimation of long-period variability of the Mars atmospheric constituents.

2.2. Precise Orbit Determination

The estimation of the Martian atmospheric density variability, as well as the recovery of the Mars gravity field, requires precise orbit determination of the MRO spacecraft. At NASA GSFC, the orbit determination of MRO is performed using the GEODYN II Orbit Determination and Geodetic Parameter Estimation software [*Pavlis et al.*, 2013]. The MRO tracking data, both range and range rate, are processed dynamically in 1 or 2 day arcs by means of a batch least squares filter [*Tapley et al.*, 2004]. We divide the data into arcs (a continuous span

of time) in order to minimize the buildup of errors caused by the mismodeling of forces. In general, arc length is a compromise between increased sensitivity with respect to parameters, and this error buildup. The parameters that are estimated are divided into two sets: arc parameters, which affect only measurements within an arc (e.g., the initial state and the drag parameter C_D), and common parameters, which affect all measurements (e.g., gravity parameters and atmospheric parameters). First, the arc parameters are determined through iteration using batch least squares. Once this is converged, the partial derivatives of all parameters (including the common parameters) are generated. Then, the normal equation system per arc is formed, and all systems are added into the final normal equation system, which is then solved, yielding the final estimates of the common parameters. Arc parameters can be solved simultaneously, or they can be solved implicitly by taking into account their Schur complement [*Demmel*, 1997]. The least squares technique consists in the adjustment of the estimation parameters in order to minimize the observation residuals (e.g., discrepancies between observed and predicted values).

In order for GEODYN to accurately obtain the computed observables (predictions), the measurement models include tropospheric and ionospheric delays, Earth orientation parameters (supplied by the International Earth Rotation Service [*Gambis*, 2004]) and ocean loading corrections. We carefully modeled all the satellite forces, with particular emphasis on gravitational, radiation pressure, and atmosphere drag. The Mars geopotential U is modeled as a spherical harmonic expansion [*Kaula*, 1966] as follows:

$$U = \frac{\mathrm{GM}}{r}\left\{1 + \sum_{l=2}^{m}\left(\frac{a_e}{r}\right)^l \sum_{m=0}^{l}[\bar{C}_{lm}\cos m\lambda + \bar{S}_{lm}\sin m\lambda]\bar{P}_{lm}(\sin\phi)\right\} \quad (1)$$

where GM is the planetary gravitational constant, r, λ, and ϕ are the body-fixed coordinates of radial distance, longitude, and latitude, respectively, the a_e is the reference equatorial radius, $\bar{P}_{lm}$ are the normalized associated Legendre functions of degree l and order m, and $\bar{C}_{lm}$ and $\bar{S}_{lm}$ are the normalized spherical harmonic coefficients. In our analyses, we used the MROMGM0032 model that provides the Mars gravity field to degree and order 95 [*Lemoine and Mazarico*, 2009]. The model includes 2 years of MRO data (from August 2006 to August 2008), 6 years of Mars Odyssey data (from 2002 to 2008), and the entire set of MGS. The reference radius was set to 3396.0 km, and the coordinate system was based on a more complete Mars orientation model with nutation recovered by *Konopliv et al.* [2006] from MGS and Mars Odyssey tracking data. The gravitational potential also includes modifications due to tides caused by the Sun and Phobos and seasonal CO_2 cycle. The tidal potential is expressed in terms of the Love number $k_2 = 0.17645$ as determined by *Konopliv et al.* [2011]. The seasonal signal is modeled as a harmonic variation of the $\bar{C}_{20}$ and $\bar{C}_{30}$ expected functional form [*Konopliv et al.*, 2006; *Zuber et al.*, 2007; *Konopliv et al.*, 2011]. The positions of Mars, Phobos and Deimos, are obtained from the Jet Propulsion Laboratory ephemerides DE421 [*Folkner et al.*, 2009] and MAR085 [*Jacobson*, 2010] and are required for third-body perturbations and Doppler and range processing.

The modeling of the nonconservative forces is critical to the orbit determination of MRO, as they significantly affect its trajectory. The three major forces that act on the spacecraft are the atmospheric drag, the solar and planetary radiation pressure, and the spacecraft thrusts used to desaturate the angular momentum wheels (called Angular Momentum Desaturation maneuvers or AMDs). The MRO AMDs happened every day for the first few months of the mission, but only every 2 days after November 2006. For this reason, we chose arc lengths of 1 or 2 days in order to exclude the AMDs from the solutions. To compute the effects of radiation pressure and drag, the spacecraft is modeled as a set of plates representing the spacecraft bus, the solar panels, and the antenna. The orientation of each plate is determined from spacecraft telemetry and the specular and diffusive coefficients for each plate are based upon combination of surface types [*You et al.*, 2007]. The MRO panel reflectivities and the scaling factor for the solar pressure force ($C_R = 1$) are not estimated.

A more precise computation of the spacecraft cross-sectional areas for the radiation pressure and the atmospheric drag is achieved by accounting for the interplate self-shadowing of the spacecraft physical model [*Mazarico et al.*, 2009]. The consideration of self-shadowing significantly improves the fidelity of both solar radiation pressure and drag accelerations. The large size of the MRO high-gain antenna, necessary to transmit the large amount of data, leads to significant self-shadowing in the Sun and velocity directions. The modeling of the self-shadowing for the atmospheric drag force on MRO is particularly important for our purposes, since the discrepancies in the drag acceleration with and without self-shadowing can be up to 1×10^{-8} m/s^2 [*Mazarico et al.*, 2009].

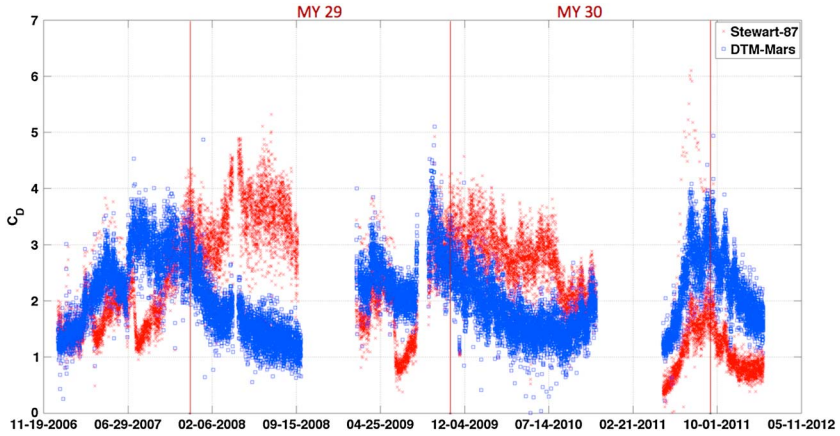

Figure 2. MRO atmospheric drag coefficients (C_D) during the first 6 years of the mission that cover four Martian Years (MY) between 28 and 31. Red and blue dots represent the C_D determined with Stewart-87 and DTM-Mars models, respectively. The vertical red lines correspond to 0° areocentric longitude.

The atmospheric drag acceleration is given by the following expression:

$$a_{\text{drag}} = \frac{1}{2}\frac{\rho C_D V^2}{m}\sum_i A_i \mathbf{n_i}\cdot\mathbf{n_V} \tag{2}$$

where C_D is the aerodynamic drag coefficient, V is the spacecraft velocity, $\mathbf{n_V}$ the along-track vector, A_i and $\mathbf{n_i}$ the surface area and normal vector for each of the macro model plates, and m the mass of the spacecraft. The lateral wind and aerodynamic lift are neglected in this study. A semiempirical density model, Stewart-87 [*Stewart*, 1987], has been previously included in our orbit determination program to predict the density ρ along the spacecraft trajectory. The atmospheric drag model has been recently updated to use density values (ρ) from the DTM-Mars model, which is described in detail in section 3. The main advantage of including this semiempirical atmospheric model in our orbit determination software is the possibility not only to have better predictions of atmospheric density and temperatures but also to enable the direct estimation of its coefficients. The DTM-Mars model is based on the assumption of diffusive equilibrium of the atmospheric constituents in the upper atmosphere, so the total atmospheric density ρ is the sum of the partial densities of the different species. Each partial density is the sum of the terms that include both short- and long-term periods, which are defined in detail in section 3. The coefficients that quantify the variability of the major atmospheric constituents appear explicitly in the atmospheric drag acceleration, so the computation of the partial derivatives of the spacecraft acceleration with respect to the DTM-Mars coefficients is straightforward. Following the procedure outlined at the beginning of this section, the atmospheric parameters are determined as the common parameters from a series of arcs covering the whole data span (~7 years).

We also adjusted the drag aerodynamic coefficient, once per orbit, to mitigate perturbations that are not included in the DTM-Mars model, such as the dust storms. The spacecraft aerodynamic drag coefficient, which depends especially on the shape of the spacecraft, is known with an accuracy of ~4.5% [*Tolson et al.*, 2008]; therefore, its correction is used to empirically scale the atmospheric density. The MRO C_D over the range of expected densities for flow along the along-track direction is between 1.7 and 2.3 [*Tolson et al.*, 2008]. To ensure smooth variations between C_D estimates over adjacent orbital periods, we applied time correlation constraints on the C_D of the same arc. *Rowlands et al.* [2010] and *Lemoine et al.* [2013] already used spatial and temporal constraints for mascon parameters (Gravity Recovery and Climate Experiment mission) and orbital accelerations (Gravity Recovery and Interior Laboratory mission), respectively. The weight assigned to the constraint equations is defined as

$$W_{ij} = S \times \exp\left(1 - \frac{t_{ij}}{T}\right) \tag{3}$$

where W_{ij} is the weight given to the constraint between two parameters i and j, $S = 1/\sigma_A^2$, σ_A is the sigma assigned to control the amplitude of the estimated parameters, t_{ij} is the difference in time between the two time tags of the two parameters i and j, and T is the correlation time. We chose this later parameter to be one orbital revolution (112 min), σ_A was set to be 0.1, and the a priori uncertainty on the single C_D is equal to 10. Figure 2 shows a comparison of the time series of the drag coefficients estimated in the POD process

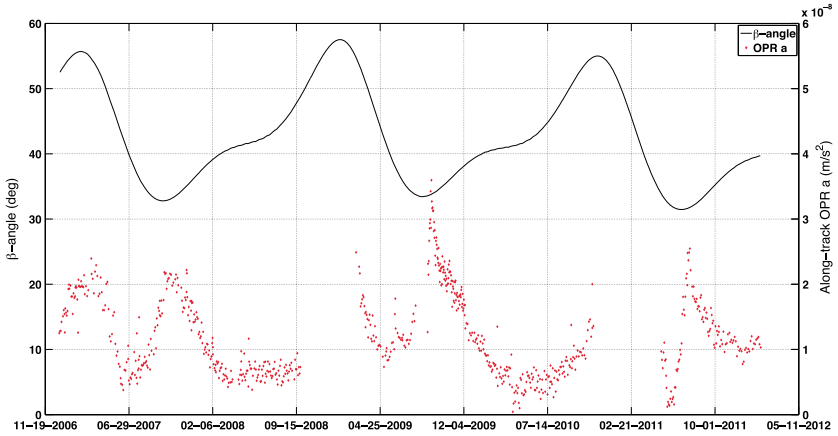

Figure 3. Total amplitude of the OPR along-track accelerations (red dots) and β angle (blue line) during the MRO mission. The accelerations show maximum values at minimum β angles, absorbing especially solar radiation pressure mismodeling.

using densities from the a priori DTM-Mars and the Stewart-87 models. The estimation of C_D with DTM-Mars is more stable, and a trend is clearly visible during the Martian year, with maximum drag coefficients during the summer in the Southern Hemisphere (Figure S2). This trend is primarily due to inaccuracies in the annual symmetrical and seasonal terms of the thermosphere constituents of the DTM-Mars model but also due to dust storm events, which are strongest at areocentric longitudes (L_S) between 180 and 360°.

To improve the fit of the Doppler data and estimate accurately the long-term periodic atmospheric variations, we also included a set of empirical along-track once-per-revolution (OPR) periodic accelerations (cosine and sine terms) over each arc to mitigate mismodeling in the solar and planetary radiation pressure models (e.g., solar panel degradation and thermal emission of the spacecraft panels). However, these parameters tend also to absorb mismodeling of the higher harmonic coefficients of the gravity field and errors in the model density values. Therefore, we applied an a priori uncertainty on these accelerations (both sine and cosine terms) of 1×10^{-6} m/s^2. Figure 3 shows the total amplitude of the along-track OPR accelerations per each arc in our POD solution. The amplitude of these accelerations is on average $\sim 1 \times 10^{-8}$ m/s^2; they are relatively stable when the β angle (angle between the orbit plane and the vector from the Sun) is larger than 40° but reach a maximum (3×10^{-8} m/s^2) at minimum solar incidence angle. The drag acceleration induced on the spacecraft is always larger than the OPR accelerations, up to 2 orders of magnitude during some periods of the Martian year (Figure S3). The sine and cosine terms of the OPR accelerations help absorb mismodeled variations of the drag forces due to local time or latitudinal variability of the atmospheric density. MRO is in a Sun-synchronous orbit; therefore, latitudinal and local time terms are strongly correlated, and they cannot be well determined in this analysis. We did not use any constant term of these accelerations in order not to absorb mismodeling in the annual and semiannual variations of the partial densities of the atmospheric constituents (section 3). Furthermore, we did not include any cross-track OPR accelerations in our POD solution in order to limit the number of estimation parameters. The solar radiation pressure slightly perturbs the orbit of the spacecraft in this direction, and the cross-track accelerations can absorb this mismodeling at certain orbit geometries. Nevertheless, the atmospheric solution does not show any significant change when those accelerations are incorporated.

From the total 968 converged arcs in total for our radio tracking data analysis of MRO, from August 2006 to January 2012, we downselected 748 arcs by excluding all the arcs that occurred during superior solar conjunctions (Sun-Earth-Probe angle $< 20°$). The selected arcs are included in a global solution focused on the estimation of the annual symmetrical and seasonal variability of the major constituents of the Martian atmosphere at the MRO altitudes such as CO_2, O, and He.

3. Mars Upper Atmosphere Modeling

The Mars upper atmosphere is conventionally partitioned into a thermosphere that is the region above 100 km, where the temperature increases with increasing altitude, and an exosphere. The MRO periapse is located just above the boundary, called exopause, that delimits these two regions. The temperature and

density of the upper atmosphere are regulated by the energy input from solar Extreme ultraviolet (EUV) absorption, and the diffusive separation of individual gases [*Barth et al.*, 1992]. The solar cycle, Martian seasons, the upward energy propagation from the turbulent lower atmosphere, and the fluctuating amount of dust in the atmosphere all further contribute to variability [*Bougher and Shinagawa*, 1998; *Bougher et al.*, 2000]. These mechanisms have only been partially characterized by the in situ and remote sensing measurements, primarily because of the limited coverage in space and time [*Keating et al.*, 1998; *Valeille et al.*, 2009a].

MGS, Mars Odyssey, and MRO accelerometer experiments, conducted during the aerobraking phase, contributed to improve the understanding of the density structure and variability of the upper atmosphere up to 160 km altitude [*Withers*, 2006; *Mazarico et al.*, 2007b; *Tolson et al.*, 2008]. However, the atmospheric drag effects on the spacecraft outside of aerobraking have rarely been considered as an indirect measurement of the atmospheric density [*Tracadas et al.*, 2001; *Lemoine et al.*, 2001; *Mazarico et al.*, 2007a]. *Bruinsma and Lemoine* [2002] explicitly used the MGS radio tracking data to determine density profiles of the exosphere at ~400 km. In general, the density structure of the upper thermosphere (above 170 km) and the exosphere substantially relies on models that propagate upward atmospheric temperature and density measured at lower altitudes.

Thermospheric models are fundamental to quantify the atmospheric loss to space and the evolution of the planet. General circulation models have been involved in interpreting data from Mars missions to study the climate of Mars in the long term [*Bougher et al.*, 1990; *Justus et al.*, 2006; *Yagi et al.*, 2012; *Chaufray et al.*, 2015]. Moreover, a good knowledge of atmospheric density at high altitudes is critical to lander entry, and to orbiter operations and lifetime. In the orbit determination process of NASA spacecraft that orbit around Mars, the atmospheric density drag model is generally based on the semianalytical Stewart model, developed by *Stewart* [1987] at the Laboratory for Atmospheric and Space Physics at the University of Colorado, or the tabulated Mars-GRAM, which is based on the NASA Ames Mars general circulation model below 80 km altitude, and on the University of Arizona Mars thermospheric general circulation model (MTGCM) from 80 to 170 km [*Justus et al.*, 1996, 2006]. At higher altitudes, the Mars-GRAM 2010 model still uses a modified Stewart thermospheric model, in particular for the dependence on solar activity. The lack of data on the total atmospheric density and partial densities of key species above 200 km substantially affects the accuracy of both models [*Bruinsma and Lemoine*, 2002]. Figure 4 shows a latitude-local time map of the predicted densities from the a priori DTM-Mars, Stewart-87, and Mars-GRAM 2010 models at 255 km altitude, for $L_S = 90°$ and a mean flux of 65 solar flux units (sfu). The former model does not provide an adequate representation of seasonal and diurnal variations of the atmospheric density, whereas Mars-GRAM 2010 and DTM-Mars are much more consistent.

The Stewart atmosphere model has been previously included into the NASA/GSFC GEODYN II orbit determination program to process the tracking data of Mars orbiters such as MGS [*Lemoine et al.*, 2001], Mars Odyssey [*Mazarico et al.*, 2007a, 2007b], and MRO. The recovery of the Mars seasonal gravity field requires an accurate prediction of atmospheric density because of MRO's periapse altitude of 255 km, which leads to strong drag forces. Therefore, we developed an enhanced semiempirical DTM-Mars model to adequately predict the temperature, and partial density variations along the MRO trajectory.

DTM-Mars predicts density and temperatures as a function of position (altitude, latitude, and local solar time), solar activity, and season. The function that provides short- and long-period variabilities of temperatures and partial densities is given by

$$G_i = A_1 + A_2 + \mathrm{SA}_1 + SA_2 + \mathrm{MSA} + \mathrm{LT} + \mathrm{LAT} \tag{4}$$

where *i* is equal to 138 and *inf* in the case of temperature variability at the lower boundary of the thermosphere and at the thermopause, respectively, or *i* is equal to CO_2, CO, O_2, O, N_2, Ar, CO, He, H_2, and H, in the case of partial density variability of those species. A_1, A_2, SA_1, and SA_2 provide periodic and seasonal variations due to the eccentric Mars orbit around the Sun that generates annual ($P = 686.971$ days) and semiannual terms, and the other three terms reproduce variations as a function of mean solar activity (MSA), local time (LT), and latitude (LAT). The terms A_1 and A_2 are respectively the symmetrical annual and seasonal annual variabilities, which are given by

$$\begin{aligned} A_1 &= (a_1 + a_2 P_{20} + a_{19} F)\cos(\Omega t) + (a_3 + a_4 P_{20} + a_{20} F)\sin(\Omega t) \\ A_2 &= (a_5 P_{10} + a_6 P_{30} + a_7 P_{50})\cos(\Omega t) + (a_8 P_{10} + a_9 P_{30} + a_{10} P_{50})\sin(\Omega t) \end{aligned} \tag{5}$$

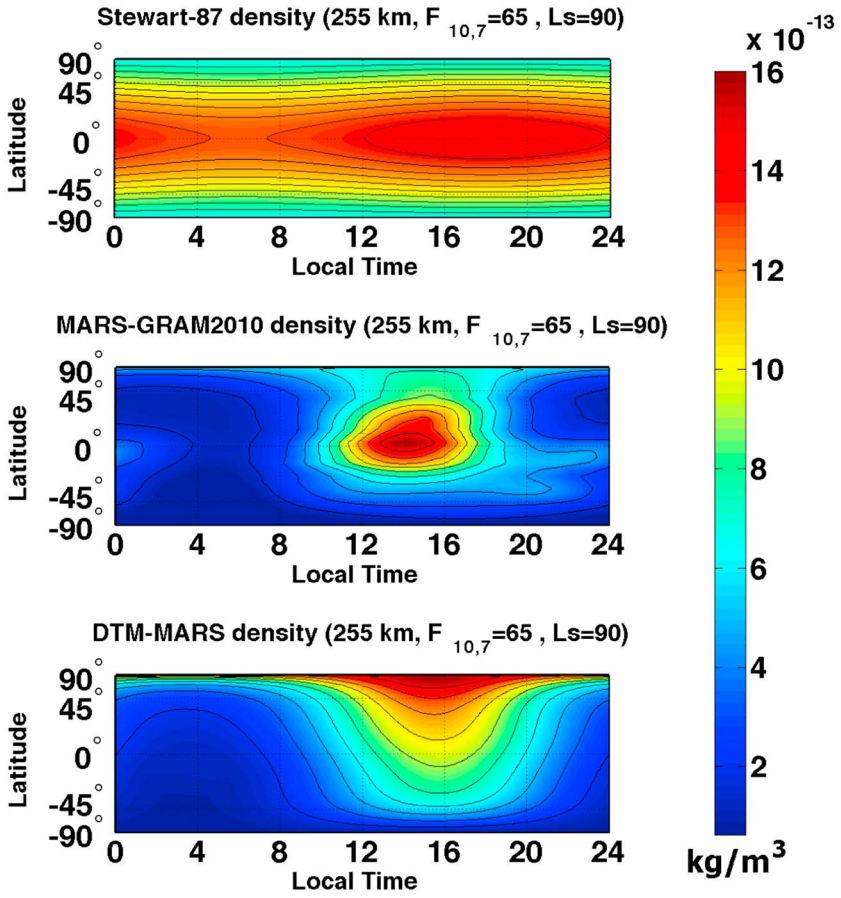

Figure 4. Predicted densities of Stewart-87, Mars-GRAM 2010, and DTM-Mars at 255 km altitude, for $L_S = 90°$ and a mean flux of 65 sfu in a latitude versus local time grid.

The symmetrical semiannual (SA_1) and seasonal semiannual (SA_2) variability terms are

$$\begin{aligned} SA_1 &= (a_{11} + a_{12}P_{20} + a_{21}F)\cos(2\Omega t) + (a_{13} + a_{14}P_{20} + a_{22}F)\sin(2\Omega t) \\ SA_2 &= (a_{15}P_{10} + a_{16}P_{30})\cos(2\Omega t) + (a_{17}P_{10} + a_{18}P_{30})\sin(2\Omega t) \end{aligned} \tag{6}$$

and the MSA, LT, and LAT are as follows:

$$\begin{aligned} \mathrm{MSA} &= a_{23}F \\ \mathrm{LT} &= (a_{24}P_{11} + a_{25}P_{21} + a_{26}P_{31})\cos(\omega t) + (a_{27}P_{11} + a_{28}P_{21} + a_{29}P_{31})\sin(\omega t) \\ \mathrm{LAT} &= a_{30}P_{10} + a_{31}P_{20} + a_{32}P_{30} + a_{33}P_{40} + a_{34}P_{50} \end{aligned} \tag{7}$$

where a_i are a set of coefficients that can be estimated for each species or temperature, Ω is the mean angular velocity of the orbit of Mars around the Sun ($2\pi/659355072$ rad/s), and ω is the rotational angular velocity of Mars ($2\pi/88668$ rad/s). These periodic variations depend on the latitude by means of unnormalized associated Legendre functions P_{nm} of degree n and order m, and the atmospheric heating process due to the solar electromagnetic radiations ($F = \bar{F}_{10.7} - 65$), related to the intensity of the solar EUV and UV emissions characterized by the 10.7 cm flux ($\bar{F}_{10.7}$) at Mars.

The model is based on the hypothesis of independent static diffusive equilibrium of different atmospheric constituents: CO_2, CO, O_2, O, N_2, Ar, CO, He, H_2, and H as adopted in previous thermospheric models [*Bruinsma and Lemoine*, 2002]. The partial density of each constituent, given at 138 km, is propagated upward fulfilling the $f_i(z)$ altitude law. The total density is defined as the sum of the partial densities of each constituent as follows:

$$\rho(z) = \sum_i \rho_i^{138\mathrm{km}} f_i(z)\exp(G_i) \tag{8}$$

where $\rho_i^{138\mathrm{km}}$ is the partial density of each constituent at 138 km, the spherical harmonic function G_i reproduces periodic and nonperiodic variations per each constituent i. The $f_i(z)$ altitude law relies on the altitude

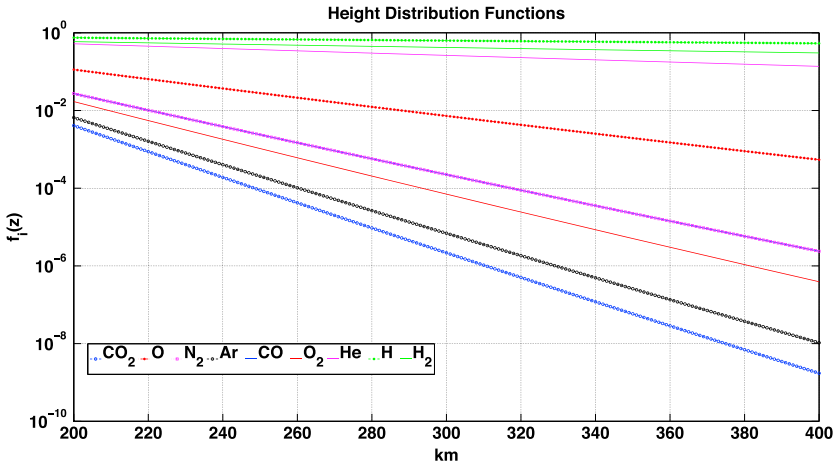

Figure 5. Exponential height distribution functions $f_i(z)$ with respect to the altitude above the surface for each atmospheric constituents (CO_2, CO, O_2, O, N_2, Ar, He, H_2, and H). These curves are plotted considering constant $T^o_{inf} = 226.93$ K and $T^o_{138} = 169.76$ K, which evolve in our model depending on season, local solar time, latitude, and also as function of the atmospheric heating process due to the solar electromagnetic radiations and because of the particle flow.

z with respect to the spheroid of radius 3376.87 km, the thermopause temperature T_{inf}, and the temperature T_{138} at 138 km (lower limit of the model). This function, reported explicitly in *Bruinsma and Lemoine* [2002], is retrieved by the integration of the differential equations of diffuse equilibrium and uses the Bates temperature profile [*Bates*, 1959]. The altitude law depends explicitly on T_{inf}, and T_{138}, which are defined as $T_i = T^o_i(1 + \exp(G_i))$, where the initial temperatures (T^o_{138}, T^o_{inf}) and the coefficients of the functions G_{138} and G_{inf} were determined by *Bruinsma and Lemoine* [2002] using Mars-GRAM 2000 and MTGCM results [*Bougher et al.*, 2000]. Figure 5 shows the altitude law profiles for each atmospheric constituent.

This model can also take into account the effect of a global dust storm on the atmospheric temperatures and densities with a representation similar to the Stewart-87 model [*Stewart*, 1987]. Although the inclusion of a dust storm perturbation can help predict the atmospheric conditions, this modeling is generally not accurate enough because of the high variability of dust storm timing and intensity during different Martian years. For this reason, we used other tools (i.e., drag coefficients) to absorb dust storm perturbations.

The coefficients of the a priori model that define CO_2, O, and He partial densities were retrieved from the analysis of MGS accelerometer and radio tracking observations [*Bruinsma and Lemoine*, 2002], whereas the other atmospheric constituents partial densities are based on Stewart-87. *Bruinsma and Lemoine* [2002] derived some of the coefficients of the Mars-DTM from MGS accelerometer observations during the aerobraking phase and from the analysis of precise orbit determination results during the mapping phase. Therefore, the DTM-Mars describes accurately the helium periodicity as a function of solar activity and day of year. Furthermore, the MGS aerobraking phase provided accelerometer data from 140 to 160 km altitudes that allowed the determination of the annual variation of CO_2. However, the lack of an adequate data coverage (accelerometer collected measurements at $41° < L_S < 86°$ and $214° < L_S < 301°$) lead to possible errors in the prediction of the Mars atmosphere density at MRO periapsis altitude, especially for CO_2 and O. Along MRO's orbit, the dominant species alternate between CO_2, O, and He. Atomic oxygen commonly makes up about 70–80% of the total density at altitudes lower than 300 km as confirmed by data from the Mars-GRAM2010 and the a priori DTM-Mars models. *Valeille et al.* [2009a] showed that CO_2 is comparable to O at altitudes near 190 km, and their local distribution relies strongly on latitude. At these altitudes, atomic oxygen has maximum densities at low latitudes on the nightside and at the pole during the winter when temperatures are lower, and carbon dioxide densities are larger where temperatures are warmer [*Valeille et al.*, 2009b]. Although the MRO periapsis altitude is higher than the altitude where CO_2 and O have similar abundances, data from Mars-GRAM2010 and the a priori DTM-Mars models showed that carbon dioxide reaches higher densities also at 255 km altitude during summer in the southern hemisphere. For this reason, we present in this work a sensitivity analysis (section 4.2) to determine the recoverability of these three constituents, finally focusing on the estimation of CO_2 and O annual and semiannual variabilities with MRO radio tracking data.

4. Results

In this section, we first report a qualitative discussion showing the criteria that led us to focus our estimation on specific coefficients of the atmospheric model. Afterward, we present the global estimation of those coefficients with the selected POD arcs. The method adopted in this work consists of a preliminary POD solution to determine the MRO orbit by estimating the local parameters, which are the spacecraft initial states, the drag coefficients, and the along-track OPR accelerations. After convergence of the orbit determination, we computed the partial derivatives of the common parameters, which here are only the atmospheric model coefficients. The collected orbital information is used to produce normal equations that are solved to yield a combined estimation of various orbital parameters, including spacecraft initial states and $C_D s$, and the coefficients of the atmospheric model that define the partial densities of the selected species.

4.1. Model Boundary Conditions

The determination of the atmospheric constituents variability relies on the temperature model, and the boundary conditions of partial densities and temperatures. The values used in our model are $\rho_{CO_2}^{138km} = 8 \times 10^{-10}$ kg/m^3, $\rho_{O}^{138km} = 1 \times 10^{-11}$ kg/m^3, and $\rho_{He}^{138km} = 4 \times 10^{-14}$ kg/m^3 for the partial densities of CO_2, O, and He at 138 km, and the temperatures 170 K and 227 K for T_{138}^{o} and T_{inf}^{o}, respectively. These initial conditions and the temperature model were obtained by *Bruinsma and Lemoine* [2002], and they are not updated or readjusted in this study because the a priori coefficients of the model, which reproduce the variability of the atmospheric partial densities, are consistent with these assumptions. However, we dedicated further tests to assess the robustness of our results by perturbing $\rho_{CO_2}^{138km}$, ρ_{O}^{138km}, ρ_{H2}^{138km}, T_{138}, and T_{inf}. We modified the boundary conditions with values from the Mars-GRAM2010 data or by scaling directly their nominal values. The main effect of these perturbed initial densities and temperatures is a change in the predictions of the total atmospheric density that is constantly scaled. However, the long-period variabilities of the atmospheric density, which is given by the function G_i, are not significantly affected, and the estimation of the DTM-Mars coefficients is stable. The constant variation of the total atmospheric density is, indeed, compensated by corrections of the drag coefficients. Figure S4 shows the estimated C_D using Mars-GRAM2010 data for the boundary conditions of partial densities and temperatures, compared to our nominal case. The $C_D s$ with the Mars-GRAM2010 initial conditions are constantly scaled to lower values that are far from the expected range of the aerodynamic coefficients (section 2.2). Similar results, which showed unreasonable drag coefficients, are also obtained by scaling directly the initial conditions of $\rho_{CO_2}^{138km}$, ρ_{O}^{138km}, ρ_{H2}^{138km}, T_{138}, and T_{inf} suggesting that their nominal values combined with the a priori coefficients of the model provide a more consistent prediction of both density and temperature at MRO altitudes.

4.2. Sensitivity Analysis

The orbital configuration of the MRO spacecraft is a major factor in the estimation of the coefficients of the DTM-Mars model. MRO is in a 255 km × 320 km near-polar orbit with the periapsis above the South Pole of Mars (82°S). At those altitudes, the a priori DTM-Mars model shows that CO_2, O, and He are the major constituents representing more than 95% of the total density. Accordingly, the coefficients that regulate the partial density of the other species are not detectable and are not adjusted in this study.

In this 65 km thick region of the Martian upper atmosphere, the dominant species in terms of partial density and thus drag on the spacecraft alternate between CO_2, O, and He. The MRO periapsis altitude is near the upper boundary of the thermosphere region where CO_2 is the most abundant species. Therefore, at MRO lower altitudes CO_2 and O are comparable and provide stronger drag perturbations on the spacecraft during its orbit. Figure 6 shows the maximum partial density of CO_2, O, and He predicted from DTM-Mars for each arc. Helium partial density has a relatively flat trend compared to the other species, and therefore, its annual and seasonal variations are not distinguishable in the MRO radio tracking data. Moreover, the abundance of He throughout the Martian year is significantly lower than O and CO_2, especially, during spring and summer in the southern hemisphere when CO_2 shows a maximum partial density more than 1 order of magnitude larger. Carbon dioxide is less abundant than O from $0° < L_S < 210°$, but it becomes the major constituent at MRO periapsis altitude during summer in the southern hemisphere reaching a partial density of $\sim 4 \times 10^{-12}$ kg/m^3.

Although the MRO orbit configuration reveals explicitly the small contribution of helium to the drag forces, we performed a preliminary covariance analysis to assess the sensitivity of the DTM-Mars coefficients and the potential to determine its variability. The estimation of He annual and semiannual coefficients leads to large values yielding unreasonable results in terms of He partial density. This effect is compensated by a dramatic

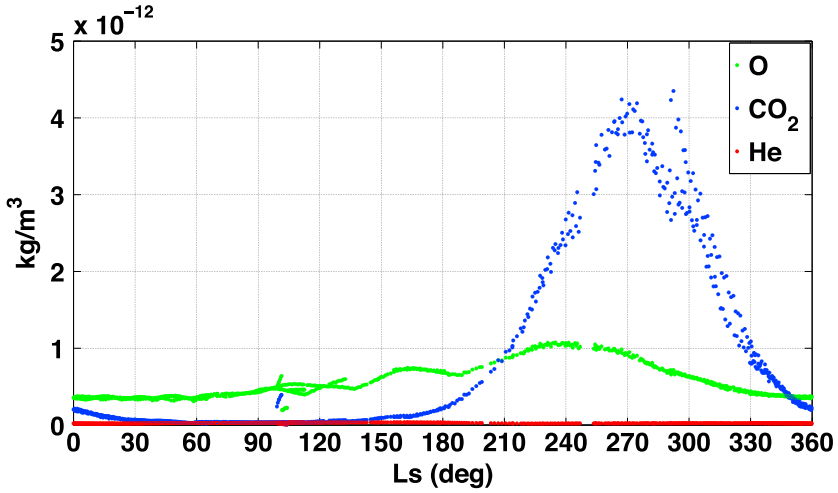

Figure 6. Maximum partial densities of the three major constituents CO_2 (blue), O (red), and He (green), predicted from DTM-Mars, along the MRO orbit in a latitude-L_S grid.

decrease of the MRO C_Ds that tend to be small (0.5–1.5 versus 1.5–3 previously). Another piece of information that helium does not influence significantly MRO orbit is reported in Figure 7. This image shows which species has the larger partial density with respect to the spacecraft orbital latitude during the Martian year. Helium is the major constituent only during the summer in the southern hemisphere at high latitudes where the spacecraft is at its apoapse and the atmospheric total density is significantly lower. The solar activity (Figure S5) affects significantly the ratio of oxygen and helium at ~300 km altitude, low solar activity leads to more abundant helium at those heights. Figure 7 also shows larger He partial density at L_S ~95° in the southern hemisphere; however, these data correspond to the aerobraking phase (August and September 2006) when the periapsis latitude was located in the northern hemisphere.

The plot of the atmospheric major constituent with respect to latitude and season highlights that MRO samples more evenly latitudinal regions where the atomic oxygen is the most abundant. Therefore, the estimation of the O model coefficients is expected to be more stable and leads to improvements not only in the symmetrical annual and semiannual predictions but also in the seasonal variations. These latter terms are, indeed, a function of latitude by means of associated Legendre functions P_{nm}. More problematic is instead the recovery of the CO_2 seasonal coefficients since the carbon dioxide provides a strong contribution on MRO drag forces only during spring and summer in the southern hemisphere. A dedicated covariance analysis allowed us to confirm that CO_2 seasonal coefficients of the DTM-Mars model are not recoverable from MRO only.

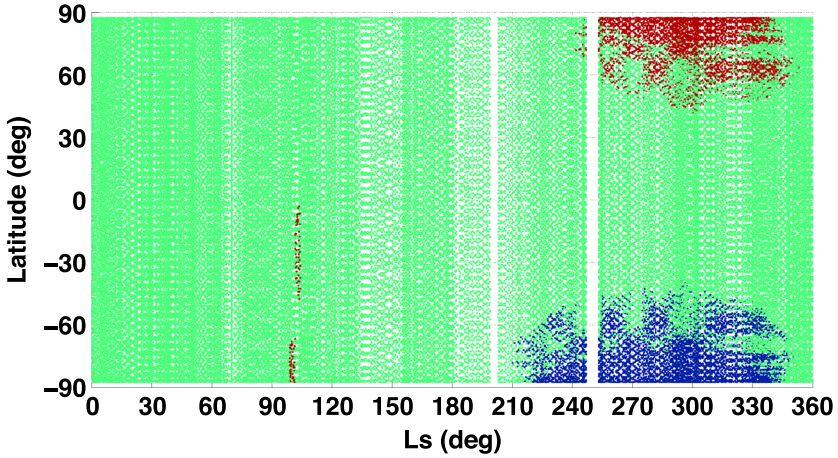

Figure 7. Latitude-areocentic longitude map that shows the local atmospheric major constituent along the MRO orbit. Blue, green, and red dots represent the locations where CO_2, O, and He are the dominant species, respectively.

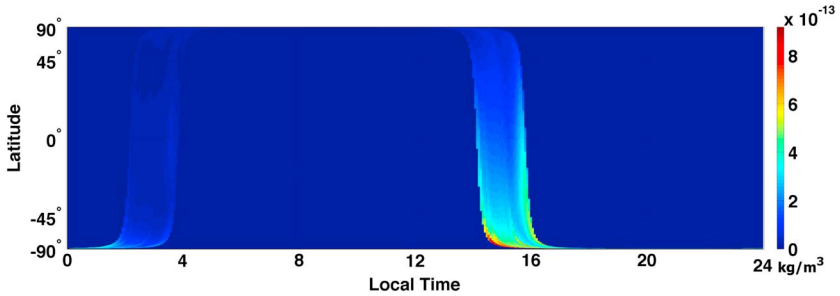

Figure 8. Latitudinal and local time map of the average atmospheric total density indirectly measured by MRO.

Another orbit configuration constraint limits the recovery of the DTM-Mars model coefficients. The Sun synchronicity of the orbit, with a local mean solar time of approximately 3 P.M., leads to atmospheric sampling of those solar longitudes only. Figure 8 shows the latitude-local time map of the mean atmospheric total density along the MRO path. The Sun-synchronous orbit covers the same latitude at approximately the same local time; therefore, we are not able to provide a reliable estimation of the DTM-Mars coefficients that define the atmospheric diurnal variation, which relies thereby on the a priori values of the model.

In conclusion, the sensitivity of the DTM-Mars model coefficients assumed from the orbital coverage limitations were confirmed from our covariance analysis results. The MRO altitude allows us to only determine the model coefficients that describe CO_2 and O long-term variability, and the Sun synchronicity of the orbit leads us to exclude the diurnal coefficients from the estimated parameters.

4.3. CO_2 and O Annual and Seasonal Variations

The MRO mission provides a long-term perspective on Mars' atmosphere variability at 250–320 km from 2006 up to the present. We analyzed the first 6 years of radio tracking data that cover three full Martian years from the end of 28 to the beginning of 31 with the goal to recover the annual and semiannual variabilities of CO_2 and O. The main challenge of the determination of CO_2 and O atmospheric model coefficients is the dust storm season that occurs during southern hemisphere summer (L_s ~210°–330°). An increased amount of dust in the lower atmosphere leads to higher atmospheric density in the upper atmosphere, a consequence of atmospheric thermal expansion due to higher solar radiation absorption in the middle atmosphere [*Bruinsma et al.*, 2013]. The DTM-Mars model has the possibility to parameterize a dust storm event as a function of dust opacity τ and time. We first used the dust optical depth retrieved from the Mars Odyssey THEMIS data [*Smith*, 2008] to simulate the effects of dust on the temperature at 138 km and the exosphere. However, the coefficients that control those temperatures as a function of the dust optical depth are not accurate enough to predict the change of the atmospheric density due to the dust loading in the atmosphere. For this reason, we did not include the dust opacity as a parameter in the atmospheric density model, and we absorb the increase of atmospheric density due to dust with the estimated drag coefficients. This approach allowed us to consider POD arcs that occurred during dust storm events ($\tau > 0.3$), especially in 2007.

The continuity of the MRO data coverage throughout the Martian year helps to accurately estimate the coefficients of the DTM-Mars as listed in Table 1. The a priori and estimated values of these coefficients and their formal uncertainties as determined in the global inversion are listed in Table 2. Both oxygen symmetrical and seasonal variations are well determined with the MRO radio science data showing comparable formal uncertainties that indicate a good level of confidence especially for the constant and offset terms. The coefficients a_5 and a_8, indeed, define the hemispherical asymmetry of the atmospheric densities with respect to the model reference frame. The lower altitudes of MRO in the southern hemisphere (~255 km at 82°S) lead to a better sensitivity to the atmospheric density over latitudes between 0°N and 90°S. As such, the better observability

Table 1. DTM-Mars Model Estimation Parameters

	Annual Variability		Semiannual Variability	
	Symmetrical	Seasonal	Symmetrical	Seasonal
CO_2	a_1 a_3		a_{11} a_{13}	
O	a_1 a_2 a_3 a_4 a_5	a_6 a_7 a_8 a_9 a_{10}	a_{11} a_{12} a_{13} a_{14}	a_{15} a_{16} a_{17} a_{18}

Table 2. Atmospheric Model Coefficients From the Final Adjusted Global Solution[a]

Constituent	Coefficients	A Priori	Estimation	Formal Uncertainty
CO_2	a_1	−0.117	0.886	0.005
	a_3	−0.559	−0.346	0.002
	a_{11}	0.089	−0.033	0.002
	a_{13}	0.001	0.236	0.002
O	a_1	−0.300	0.236	0.002
	a_2	0.000	0.197	0.003
	a_3	−0.050	0.005	0.002
	a_4	0.000	0.337	0.003
	a_5	0.000	0.271	0.001
	a_6	−0.060	−0.418	0.007
	a_7	0.000	0.265	0.010
	a_8	0.000	−0.039	0.001
	a_9	0.400	1.065	0.007
	a_{10}	0.200	−0.014	0.004
	a_{11}	0.101	0.242	0.002
	a_{12}	−0.080	−0.153	0.002
	a_{13}	−0.051	0.035	0.002
	a_{14}	0.240	−0.057	0.003
	a_{15}	0.000	0.146	0.001
	a_{16}	0.000	−0.241	0.003
	a_{17}	0.000	−0.121	0.001
	a_{18}	0.000	−0.380	0.004

[a]The a priori values are from the DTM-Mars by *Bruinsma and Lemoine* [2002].

of these two coefficients shows that the estimated model is particularly well suited to predict the O partial density in the southern hemisphere.

The geographical and seasonal distributions of CO_2 along the MRO orbit (Figure 7) does not allow an accurate determination of its seasonal variability. However, the high abundance of this species at $180° < L_s < 350°$ (Figure 6) provides significant information on the constant terms of the symmetrical annual and semiannual variabilities of carbon dioxide.

Figure 9 shows the predicted CO_2 partial densities of the a priori [*Bruinsma and Lemoine*, 2002] and adjusted DTM-Mars models, and for comparison purposes, Mars-GRAM2010 [*Justus and Johnson*, 2007; *Justh et al.*, 2011] at 255 km altitude, Local True Solar Time (LTST) midnight, for two different latitudes 82°S (top) and 0°N (bottom), for a mean flux of 65 sfu. The recovered carbon dioxide density is consistent with the a priori model, although a phase offset is clear at both latitudes. At the equator this offset is significant (~40°) with minimum and maximum densities at respectively L_S ~130° and L_S ~310°. The reported Mars-GRAM2010 results reflect the sparseness of CO_2 partial density data at those altitudes used for this model, since MTGCM data tables only cover altitudes of 80 to 170 km and a modified Stewart-type thermospheric model is used at higher altitudes above 170 km [*Justus and Johnson*, 2007]. The dynamics of the Martian atmosphere are poorly known above 200 km altitude, so a direct comparison of our results with other data set is not straightforward. However, the CO_2 partial densities from Mars-GRAM2010 at lower altitudes, as, for example, the upper limit of MTGCM data tables (Figure S6), show a trend very similar to our adjusted model, with minimum and maximum densities, respectively, during southern hemisphere winter and summer. The phase shift of the CO_2 annual periodicity that we measured in this work leads to a good correlation of the total density predictions between Mars-GRAM2010 and the adjusted DTM-Mars model. Figure 10 shows a comparison in a latitude-local time map of the predicted total densities from the a priori and adjusted DTM-Mars model (top and bottom), and Mars-GRAM2010 (middle) at 255 km altitude, for $L_S = 180°$ and a mean flux of 65 sfu. The updated model

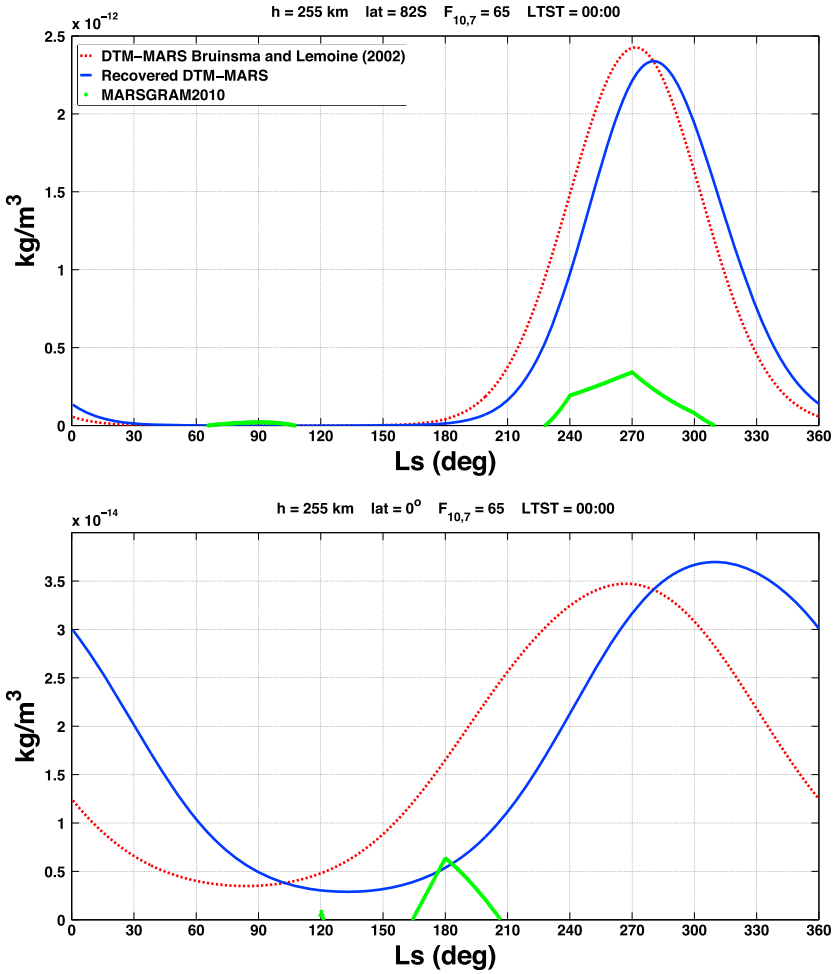

Figure 9. Carbon dioxide partial density with the a priori and adjusted model compared to Mars-GRAM2010 at 255 km altitude, LTST = 00:00, and two different latitudes (top) 82°S and (bottom) 0°N, for a mean flux of 65 sfu.

predicts lower density with respect to the a priori model and provides a global distribution more similar to the Mars-GRAM2010.

The observations of density in the upper atmosphere of Mars (between 60 and 130 km) obtained by the Mars Express ultraviolet spectrometer Spectroscopy for Investigation of Characteristics of the Atmosphere of Mars (SPICAM) are a good basis of comparison for the annual variability of CO_2 [*Forget et al.*, 2009]. The atmospheric densities observed by SPICAM [see *Forget et al.*, 2009, Figure 4] show a significant seasonal variation that is consistent with the evolution of CO_2 reported in Figure 9. The minimum densities are in good agreement, whereas there is an offset between the maximum densities measured by SPICAM and reported in this study.

The estimation of the atomic oxygen is more accurate because of the different scale heights above the homopause. Figure 11 shows the predicted O partial densities of the a priori [*Bruinsma and Lemoine*, 2002] and adjusted DTM-Mars models, and Mars-GRAM2010 [*Justus and Johnson*, 2007; *Justh et al.*, 2011], with the same conditions as in Figure 9. The adjustments in the seasonal and symmetrical semiannual terms lead to a slower decrease of the atomic oxygen in the southern hemisphere at L_S ~330°. Furthermore, this change leads to higher values of the O partial density during southern hemisphere summer at equatorial latitudes that better match the Mars-GRAM 2010 values. However, this latter model predicts minimum densities at the end of the southern hemisphere winter, which is not observed with either the a priori or adjusted DTM-Mars, which show larger values at those areocentric longitudes.

4.4. Model Validation

An indicator that provides valuable information on the quality of the estimated DTM-Mars model is the MRO drag coefficient (C_D). This coefficient absorbs discrepancies between actual and predicted values of the

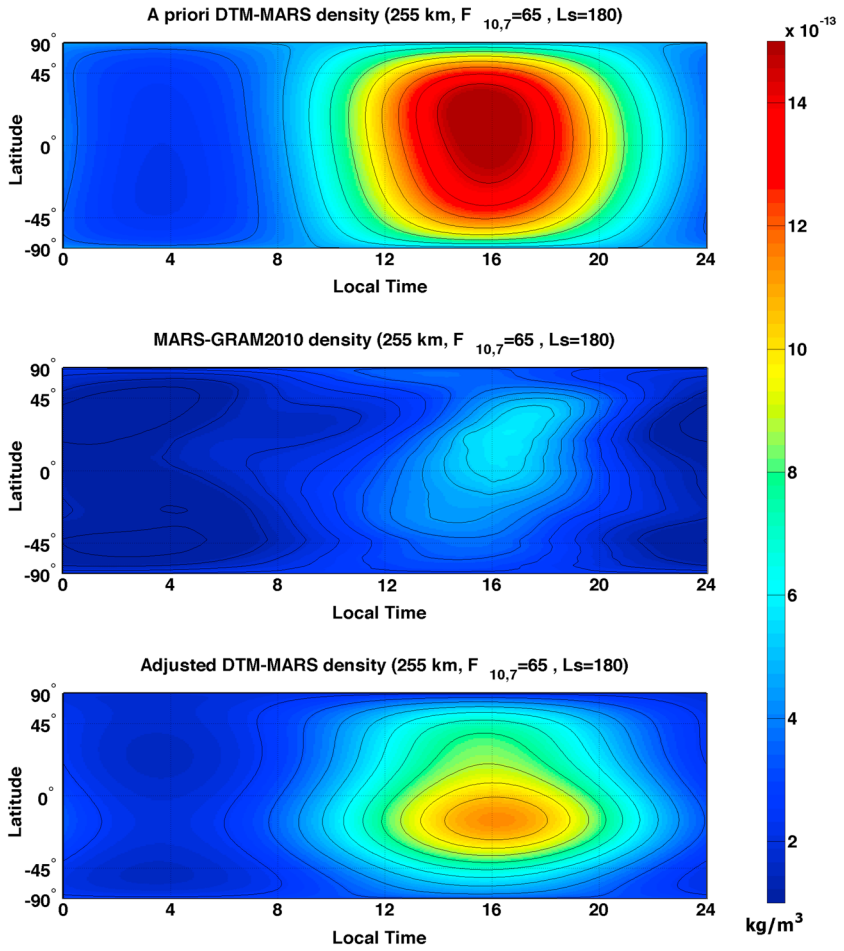

Figure 10. Predicted densities of (top) a priori and (bottom) adjusted DTM-Mars, and (middle) Mars-GRAM2010 at 255 km altitude, for $L_S = 180°$ and a mean flux of 65 sfu in a latitude versus local time grid.

atmospheric density. In this study, the DTM-Mars model does not include dust storm events; therefore, the C_D should compensate for the increase of the atmospheric density because of dust. The a priori model shows a C_D trend that follows closely seasonal long-term periodicity with maximum values during summer in the southern hemisphere. The global estimation of CO_2 and O annual and semiannual variabilities allowed us to recover that signal in a correction of the DTM-Mars coefficients.

Figure 12 shows the MRO atmospheric drag coefficients (one per orbit), after the estimation of the atmospheric model, compared to the THEMIS dust optical depth (τ) at 1075 cm^{-1} scaled to an equivalent 6.1 mbar pressure surface to remove the effect of topography [*Smith*, 2008] and computed at the reference epochs of the MRO POD arcs using data only in the southern hemisphere. The correlation between C_D and τ increases up to ~0.8 after the global estimation, compared to ~0.4 obtained with the a priori model. Although the THEMIS data do not cover evenly the latitudes near the MRO periapse, the correlation between these two parameters is good and confirms a significant improvement in the prediction of the atmospheric density with the updated DTM-Mars. Moreover, the C_D residual increase due to dust storms could provide information on the associated atmospheric temperature variations that basically correlate with the scale height of the model.

A further validation test of the recovered atmospheric model is its application in the orbit determination of an independent MRO data set, from January 2012 to April 2013. This additional year of radio tracking data does not cover a full Martian year and lacks data during the southern hemisphere summer because of a superior solar conjunction. Because these data do not cover evenly the Martian seasons, we did not include those arcs in the solution, but they proved beneficial as a test case of our results.

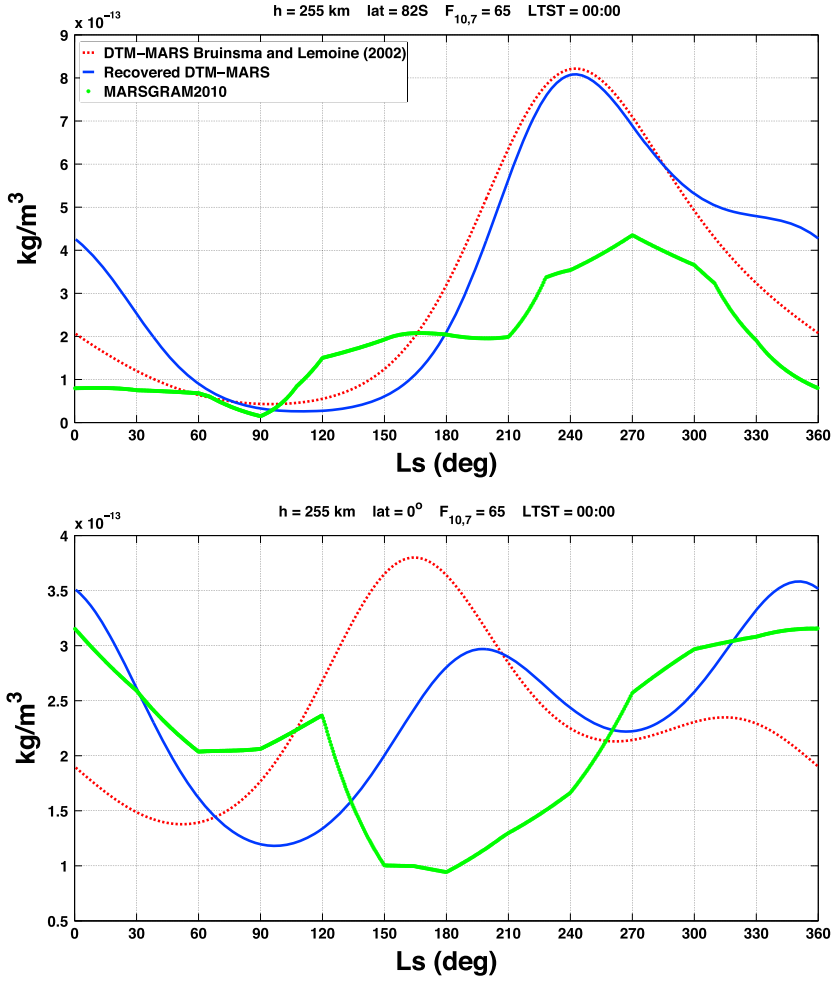

Figure 11. Atomic oxygen partial density with the a priori and adjusted model compared to Mars-GRAM2010 at 255 km altitude, LTST = 00:00, and two different latitudes (top) 82°S and (bottom) 0°, for a mean flux of 65 sfu.

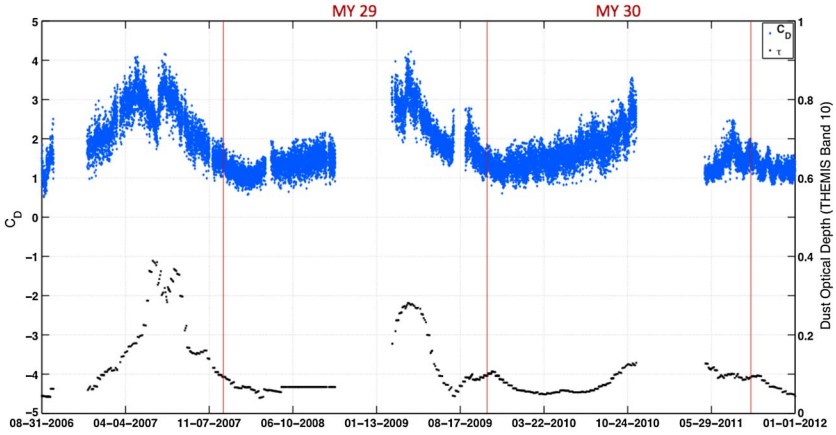

Figure 12. MRO atmospheric drag coefficients (C_D) and dust optical depth at 1075 cm^{-1} from THEMIS [*Smith*, 2008] at the reference epochs of the MRO POD arcs. The vertical brown lines correspond to $L_S = 0°$.

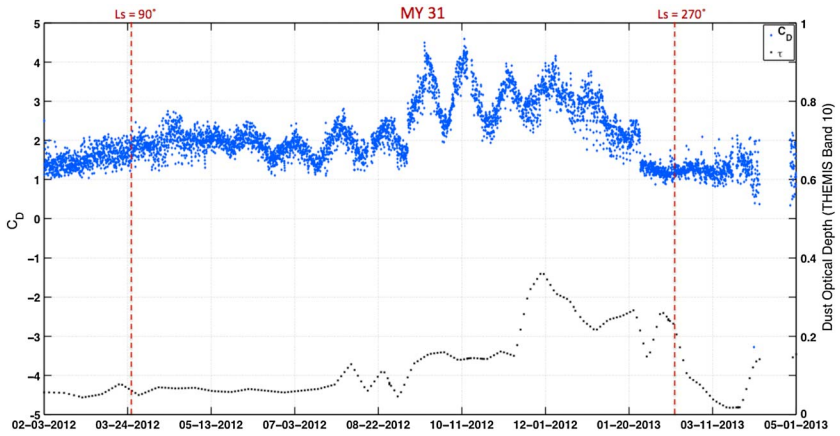

Figure 13. MRO atmospheric drag coefficients (C_D) and dust optical depth at 1075 cm^{-1} from THEMIS [*Smith*, 2008] during an additional year of MRO data, independent of the data used in the determination of the coefficients. The vertical brown dashed lines correspond to $L_S = 90°$ and 270° of the Martian Year 31.

Comparing the updated DTM-Mars to the a priori, both C_D and OPR accelerations significantly improve in the orbit determination results. The use of the a priori DTM-Mars leads to lower C_Ds (< 1.5) especially during southern hemisphere fall and winter. Figure 13 shows that the updated model provides more reasonable drag factors, which are in the range of confidence when the dust opacity is low, and increase drastically when the dust optical depth is larger than 0.1. The oscillation of dust content in the Martian atmosphere, registered by THEMIS in August 2012, is especially interesting, showing high correlation with the MRO C_D. Furthermore, another piece of information that the updated DTM-Mars version provides a better prediction of atmospheric density is that the OPR along-track accelerations required in the POD process decrease. Figure S7 shows the ratio of the total amplitude of those accelerations with the two models (a priori/updated). The accelerations with the a priori model are slightly lower for the first month of data but, afterward, they are larger from March 2012 to April 2013 up to 2–2.5 times.

5. Discussion

A detailed covariance analysis showed that we are able to determine the annual, semiannual, and seasonal variabilities of O and CO_2 that are the major constituents at the MRO periapse altitude. Carbon dioxide is the primary ingredient of the atmosphere of Mars, and the reconstruction of its annual cycle exchange between the atmosphere and polar caps is of great interest. However, at MRO altitudes CO_2 is only occasionally the more abundant species; therefore, we could recover only its annual periodicity. The updated coefficients that regulate CO_2 long-term variability essentially provide a significant change in the phase of this periodicity with respect to the a priori DTM-Mars model showing a better agreement with other measurements as, for example, density profiles from Mars Express SPICAM.

Atomic oxygen generally accounts for ~70% of the total density along the MRO orbit. The higher partial density of this species allows us to estimate both symmetrical and seasonal variations of this constituent. The O abundance at 250–350 km is important to determine temperature profile, composition, and dynamics of the Martian upper thermosphere and exosphere. However, the lack of measurements of atomic oxygen distribution limits significantly the predictability of both atmospheric density and temperature. Therefore, our results of the O annual and semiannual variabilities provide advantageous information for atmospheric density profiles at those altitudes. From this, one is able to improve general circulation models, which already suitably represent lower altitudes in the atmosphere.

The results reported in this paper depend on densities and temperatures at the boundaries of the region where the model is valid. The initial conditions adopted in our model were determined by *Bruinsma and Lemoine* [2002], solving in a least squares filter these coefficients with data from Stewart-87 and Mars-GRAM2000 models. Although these two models are not recent, the density at 138 km, and the boundary temperatures are consistent with the latest data provided by Mars-GRAM2010 model. Furthermore, we tried to retrieve the densities of CO_2, O, and He at 138 km including these parameters in the final step of our

estimation process. However, the high correlation with the drag coefficients significantly affects the stability of these solutions. For this reason, the study presented in this paper shows only the recovery of the long-term variability of the dominant atmospheric species that are sufficiently uncorrelated with other parameters such as C_Ds and along-track OPR accelerations.

6. Conclusions and Future Work

The 7 years of MRO radio science data we analyzed allowed us to provide useful information on the dynamics of the Martian upper atmosphere between 255 and 320 km altitudes. The low altitude of the spacecraft has always been considered an advantage in determination of the high degrees of the Mars gravity field but is also a significant limitation in the seasonal monitoring of the polar caps that started with MGS and continued with Mars Odyssey. The MRO periapse altitude leads, indeed, to uncompensated drag forces, whose mismodeling may affect the gravity solution. However, this strong perturbation can provide measurements of the Martian atmospheric density that are directly proportional to the drag forces on the spacecraft. Therefore, we focused our study on the determination of the long-term periodicity of the atmospheric constituents in the Mars upper atmosphere with 6 years of MRO radio tracking data that cover three full Martian years.

An updated version of the semiempirical atmospheric model DTM-Mars has been presented. We included this model in our POD software in order to improve the prediction of the atmospheric densities and to directly retrieve its coefficients by means of MRO radio tracking data. The explicit dependency of the spacecraft aerodynamic drag acceleration on the coefficients of the model, which reproduce the variability of the atmospheric species, permits to estimate them in a combined global estimation with local parameters such as spacecraft initial states, C_Ds, and OPR accelerations. We have reported the solution of 7 years of MRO radio science data that provided a significant correction on the long-term periodicity of CO_2 and O.

The direct estimation of the coefficients of a semiempirical atmospheric model from radio tracking data pave the way for future work. MGS and Mars Odyssey spacecraft, for example, show good promise to retrieve the long-term periodicity of helium since both spacecraft orbits are at ~400 km altitude, where helium is the dominant species. These data will be processed to extend the validity of our updated DTM-Mars model up to 450 km.

Acknowledgments

We are grateful to Sean Bruinsma (CNES/GRGS, Toulouse, France) for encouraging this research by providing detailed information on the DTM-Mars model that made this work possible. We thank Michael Smith (NASA, GSFC) for sharing with us THEMIS measurements of the dust optical depth. We thank David Rowlands (NASA, GSFC) for his help with the GEODYN software. The data used in this paper are available at http://geo.pds.nasa.gov/.

References

Asmar, S. W., J. W. Armstrong, L. Iess, and P. Tortora (2005), Spacecraft Doppler tracking: Noise budget and accuracy achievable in precision radio science observations, *Radio Sci.*, *40*, RS2001, doi:10.1029/2004RS003101.

Barth, C. A., A. I. F. Stewart, S. W. Bougher, D. M. Hunten, S. J. Bauer, and A. F. Nagy (1992), Aeronomy of the current Martian atmosphere, in *Mars*, edited by H. H. Kieffer et al., pp. 1054–1089, Univ. of Arizona Press, Tucson.

Bates, D. R. (1959), Some problems concerning the terrestrial atmosphere above about the 100-km level, *Proc. R. Soc. London, Ser. A*, *253*, 451–462.

Berger, C., R. Biancale, M. Ill, and F. Barlier (1998), Improvement of the empirical thermospheric model DTM: DTM94—A comparative review of various temporal variations and prospects in space geodesy applications, *J. Geod.*, *72*, 161–178.

Bougher, S. W., R. G. Roble, E. C. Ridley, and R. E. Dickinson (1990), The Mars thermosphere: 2. General circulation with coupled dynamics and composition, *J. Geophys. Res.*, *95*, 14,811–14,827, doi:10.1029/JB095iB09p14811.

Bougher, S. W., and H. Shinagawa (1998), The Mars thermosphere-ionosphere: Predictions for the arrival of Planet-B, *Earth Planets Space*, *50*, 247–257.

Bougher, S. W., S. Engel, R. G. Roble, and B. Foster (2000), Comparative terrestrial planet thermospheres: 3. Solar cycle variation of global structure and winds at solstices, *J. Geophys. Res.*, *105*, 17,669–17,692.

Bowes, A. L., C. A. Halsell, M. D. Johnston, D. T. Lyons, R. E. Lock, P. Xaypraseuth, S. K. Bhaskaran, D. E. Highsmith, and M. K. Jah (2003), Primary science orbit design for the Mars Reconnaissance Orbiter mission, 13th AAS/AIAA Space Flight Mechanics Conference, Puerto Rico, contribution 03–212. [Available at http://www.space–flight.org/AAS_meetings/2003_winter/w2003_program.pdf.]

Bruinsma, S., and F. G. Lemoine (2002), A preliminary semi empirical thermosphere model of Mars: DTM-Mars, *J. Geophys. Res.*, *107*(E10), 5085, doi:10.1029/2001JE001508.

Bruinsma, S., J. M. Forbes, J.-C. Marty, X. Zhang, and M. D. Smith (2013), Long-term variability of Mars' exosphere based on precise orbital analysis of Mars Global Surveyor and Mars Odyssey, *J. Geophys. Res. Planets*, *119*, 210–218, doi:10.1002/2013JE004491.

Chaufray, J.-Y., F. Gonzalez-Galindo, F. Forget, M. A. Lopez-Valverde, F. Leblanc, R. Modolo, and S. Hess (2015), Variability of the hydrogen in the Martian upper atmosphere as simulated by a 3D atmosphere-exosphere coupling, *Icarus*, *245*, 282–294, doi:10.1016/j.icarus.2014.08.0388.

Cutting, E., G. H. Born, and J. C. Frautnick (1978), Orbit analysis for Seasat-A, *J. Astronaut. Sci.*, *26*, 316–342.

Demmel, J. W. (1997), *Applied Numerical Linear Algebra*, SIAM, Philadelphia, Pa.

Folkner, W. M., J. G. Williams, and D. H. Boggs (2009), The planetary and lunar ephemeris De 421, *JPL Interplanet. Network Prog. Rep.*, *42–178*, 1–34. [Available at http://ipnpr.jpl.nasa.gov/progress_report/42-178/178C.pdf.]

Forget, F., F. Montmessin, J.-L. Bertaux, F. Gonzalez-Galindo, S. Lebonnois, E. Quemerais, A. Reberac, E. Dimarellis, and M. A. Lopez-Valverde (2009), Density and temperatures of the upper Martian atmosphere measured by stellar occultations with Mars Express SPICAM, *J. Geophys. Res.*, *114*, E01004, doi:10.1029/2008JE003086.

Gambis, D. (2004), Monitoring Earth orientation using, space-geodetic, techniques: State-of-the-art and prospective, *J. Geod.*, *78*, 295–303, doi:10.1007/s00190-004-0394-1.

Grotzinger, J. P., et al. (2012), Mars science laboratory mission and science investigation, *Space Sci. Rev.*, *170*, 5–56, doi:10.1007/s11214-012-9892-2.

Jacobson, R. A. (2010), The orbits and masses of the Martian satellites and the libration of Phobos, *Astron. J.*, *139*, 668–679, doi:10.1088/0004-6256/139/2/668.

Justh, H. L., C. G. Justus, and H. S. Ramey (2011), Mars-GRAM 2010: Improving the precision of Mars-GRAM, paper presented at 4th International Workshop on the Mars Atmosphere: Modelling and Observations, NASA Marshall Space Flight Center, Paris, France, 8–11 Feb.

Justus, C. G., and D. L. Johnson (2001), Mars Global Reference Atmospheric Model 2001 Version (Mars-GRAM 2001): Users guide, Technical Report, NASA Marshall Space Flight Center, NASA/TM-2001-210961. [Available at http://ntrs.nasa.gov/archive/nasa/casi.ntrs.nasa.gov/20010056680.pdf.]

Justus, C. G., D. L. Johnson, and B. F. James (1996), A revised thermosphere for the Mars Global Reference Atmospheric Model (Mars-GRAM version 3.4), *NASA Tech. Memo. 108513*, National Aeronautics and Space Administration, Marshall Space Flight Center, Huntsville, Ala.

Justus, C. G., A. Duvall, and V. W. Keller (2006), Validation of Mars Global Reference Atmospheric Model (Mars-GRAM 2001) and planned new features, *Adv. Space Res.*, *38*(11), 2633–2638, doi:10.1016/j.asr.2006.07.007.

Kaula, W. M. (1966), *Theory of Satellite Geodesy*, Blaisdell Pub. Co., Waltham, Mass.

Keating, G. M., et al. (1998), The structure of the upper atmosphere of Mars: In situ accelerometer measurements from Mars Global Surveyor, *Science*, *279*, 1672–1676.

Konopliv, A. S., C. F. Yoder, E. M. Standish, D.-N. Yuan, and W. L. Sjogren (2006), A global solution for the Mars static and seasonal gravity, Mars orientation, Phobos and Deimos masses, and Mars ephemeris, *Icarus*, *182*, 23–50, doi:10.1016/j.icarus.2005.12.025.

Konopliv, A. S., S. W. Asmar, W. M. Folkner, O. Karatekin, D. C. Nunes, S. E. Smrekar, C. F. Yoder, and M. T. Zuber (2011), Mars high resolution gravity fields from MRO, Mars seasonal gravity, and other dynamical parameters, *Icarus*, *211*, 401–428, doi:10.1016/j.icarus.2010.10.004.

Lemoine, F. G., and E. Mazarico (2009), GGMRO_095A_SHA.TAB, MRO-M-RSS-5-SDP-V1.0. NASA Planetary Data System. [Available at http://pds-geosciences.wustl.edu/mro/mro-m-rss-5-sdp-v1/mrors_1xxx/data/shadr/.]

Lemoine, F. G., D. E. Smith, D. D. Rowlands, M. T. Zuber, G. A. Neumann, D. S. Chinn, and D. E. Pavlis (2001), *J. Geophys. Res.*, *106*, 23,359–23,376.

Lemoine, F. G., et al. (2013), High-degree gravity models from GRAIL primary mission data, *J. Geophys. Res. Planets*, *118*, 1676–1698, doi:10.1002/jgre.20118.

Mazarico, E., M. T. Zuber, F. G. Lemoine, and D. E. Smith (2007a), Martian exospheric density using Mars Odyssey radio tracking data, *J. Geophys. Res.*, *112*, E05014, doi:10.1029/2006JE002734.

Mazarico, E., M. T. Zuber, F. G. Lemoine, and D. E. Smith (2007b), Atmospheric density during the aerobraking of Mars Odyssey from radio tracking data, *J. Spacecr. Rockets*, *44*, 1165–1171, doi:10.2514/1.28448.

Mazarico, E., M. T. Zuber, F. G. Lemoine, and D. E. Smith (2009), Effects of self-shadowing on nonconservative force modeling for Mars-orbiting spacecraft, *J. Spacecr. Rockets*, *46*(3), 662–669, doi:10.2514/1.41679.

Pavlis, D. E., J. Wimert, and J. J. McCarthy (2013), *GEODYN II System Description*, vols. 1–5, Contractor Report, SGT Inc., Greenbelt, Md.

Rosenblatt, P., V. Lainey, S. Le Maistre, J. C. Marty, V. Dehant, M. Pätzold, T. Van Hoolst, and B. Häusler (2008), Accurate Mars Express orbits to improve the determination of the mass and the ephemeris of the Martian moons, *Planet. Space Sci.*, *56*, 1043–1053, doi:10.1016/j.pss.2008.02.004.

Rowlands, D. D., S. B. Luthcke, J. J. McCarthy, S. M. Klosko, D. S. Chinn, F. G. Lemoine, J.-P. Boy, and T. J. Sabaka (2010), Global mass flux solutions from GRACE: A comparison of parameter estimation strategies—Mass concentrations versus Stokes coefficients, *J. Geophys. Res.*, *115*, B01403, doi:10.1029/2009JB006546.

Semenov, B. V., and C. H. Acton (2007), Mars Reconnaissance Orbiter Spice Kernels V1.0, *MRO-M-SPICE-6-V1.0*, NASA Planetary Data System.

Smith, M. D. (2008), Spacecraft observations of the Martian atmosphere, *Annu. Rev. Earth Planet. Sci.*, *36*, 191–219, doi:10.1146/annurev.earth.36.031207.124334.

Sniffin, R., S. Slobin, D. Morabito, A. Bedrossian, D. Shin, and L. Paul (2000), *DSMS Telecommunications Link Design Handbook, CL 06-2686, Rev. E*, Jet Propul. Lab., Pasadena, Calif.

Stewart, A. I. F. (1987), Revised time dependent model of the Martian atmosphere for use in orbit lifetime and sustenance studies, *Final Rep. JPL PO NQ-802429*, Laboratory for Atmospheric and Space Physics, The Univ. of Colorado.

Tapley, B. D., B. E. Schutz, and G. H. Born (2004), *Statistical Orbit Determination*, Elsevier, Boston, Mass.

Taylor, J., D. K. Lee, and S. Shambayati (2006), *Mars Reconnaissance Orbiter Telecommunications, DESCANSO Design and Performance Summary Series*, Article 12, NASA JPL California Institute of Technology, Pasadena, Calif.

Tracadas, P. W., M. T. Zuber, D. E. Smith, and F. G. Lemoine (2001), Density structure of the upper thermosphere of Mars, from measurements of air drag on the Mars Global Surveyor spacecraft, *J. Spacecr. Rockets*, *45*, 511–518, doi:10.2514/1.34301.

Tolson, R., E. Bemis, S. Hough, K. Zaleski, G. Keating, J. Shidner, S. Brown, A. Brickler, M. Scher, and P. Thomas (2008), Atmospheric modeling using accelerometer data during Mars Reconnaissance Orbiter aerobraking operations, *J. Spacecr. Rockets*, *45*, 511–518, doi:10.2514/1.34301.

Valeille, A., V. Tenishev, S. W. Bougher, M. R. Combi, and A. F. Nagy (2009a), Three dimensional study of Mars upper thermosphere/ionosphere and hot oxygen corona: 1. General description and results at equinox for solar low conditions, *J. Geophys. Res.*, *114*, E11005, doi:10.1029/2009JE003388.

Valeille, A., M. R. Combi, S. W. Bougher, V. Tenishev, and A. F. Nagy (2009b), Three dimensional study of Mars upper thermosphere/ionosphere and hot oxygen corona: 2. Solar cycle, seasonal variations, and evolution over history, *J. Geophys. Res.*, *114*, E11006, doi:10.1029/2009JE003389.

Valeille, A., M. R. Combi, V. Tenishev, S. W. Bougher, and A. F. Nagy (2010), A study of suprathermal oxygen atoms in Mars upper thermosphere and exosphere over the range of limiting conditions, *Icarus*, *206*, 18–27, doi:10.1016/j.icarus.2008.08.018.

Withers, P. (2006), Mars Global Surveyor and Mars Odyssey Accelerometer observations of the Martian upper atmosphere during aerobraking, *Geophys. Res. Lett.*, *33*, L02201, doi:10.1029/2005GL024447.

Yagi, M., F. Leblanc, J. Y. Chaufray, F. Gonzalez-Galindo, S. Hess, and R. Modolo (2012), Mars exospheric thermal and non-thermal components: Seasonal and local variations, *Icarus*, *221*, 682–693, doi:10.1016/j.icarus.2012.07.022.

You, T. H., M. D. Johnston, E. Maize, and J. E. Graf (2005), *Mars Reconnaissance Orbiter Navigation Plan, JPL D-22240, MRO 31 -202, Rev. B*, 124 pp., Jet Propul. Lab., Pasadena, Calif.

You, T. H., A. Halsell, E. Graat, S. Demcak, D. Highsmith, S. Long, R. Bhat, N. Mottinger, E. Higa, and M. Jah (2007), Mars Reconnaissance Orbiter interplanetary cruise navigation, *20th International Symposium on Space Flight Dynamics*, Annapolis, Md., contribution 3–4. [Available at http://issfd.org/ISSFD_2007/Program_2007.html.

Zuber, M. T., F. G. Lemoine, D. E. Smith, A. S. Konopliv, S. E. Smrekar, and S. W. Asmar (2007), Mars Reconnaissance Orbiter radio science gravity investigation, *J. Geophys. Res.*, *112*, E05S07, doi:10.1029/2006JE002833.